

## Research and construction of geosynthetic-reinforced soil integral bridges



Fumio Tatsuoka<sup>a,\*</sup>, Masaru Tateyama<sup>b</sup>, Masayuki Koda<sup>c</sup>, Ken-ichi Kojima<sup>c</sup>, Toyoji Yonezawa<sup>d</sup>, Yoshinori Shindo<sup>d</sup>, Shin-ichi Tamai<sup>d</sup>

<sup>a</sup> Department of Civil Engineering, Tokyo University of Science, 9-13, 2641 Yamazaki, Noda City 278-8510, Japan

<sup>b</sup> Railway Technical Research Institute, Japan

<sup>c</sup> Technology Planning Department, East Japan Railway Company, Japan

<sup>d</sup> Japan Railway Construction, Transport and Technology Agency, Japan

### ARTICLE INFO

#### Article history:

Received 27 June 2015

Revised 12 March 2016

Accepted 23 March 2016

Available online 4 April 2016

#### Keywords:

Earthquake

Full-height rigid facing

Geosynthetic-reinforced soil retaining wall

GRS integral bridge

Maintenance

Tsunami

### ABSTRACT

Geosynthetic-reinforced soil (GRS) integral bridge was developed to overcome several inherent serious problems with conventional type bridges comprising a simple-supported girder (or multiple girders) supported via bearings typically by RC abutments retaining unreinforced backfill (and a pier or piers for multiple girders). The problems include: (a) relatively high construction and maintenance costs with relatively long construction time resulting from the use of bearings and massive abutment structures usually supported by piles; (b) bumps immediately behind the abutments; and (c) a relatively low stability of the girders supported by roller bearings and the approach embankment against seismic and tsunami loads. For a GRS integral bridge, a pair of GRS walls (and an intermediate pier or piers if necessary for a long span) are first constructed. After the deformation of the supporting ground and the backfill of the GRS walls has taken place sufficiently, steel-reinforced full-height-rigid (FHR) facings are constructed by casting-in-place concrete on the wall face wrapped-around with the geogrid reinforcement. Finally a continuous girder is constructed with both ends integrated to the top of the FHR facings. The girder is also connected to the top of an intermediate pier, or piers, if constructed. The background and history of the development of GRS integral bridge is described. The first four case histories, one completed in 2012 for a new high-speed train line and the other three completed in 2014 to restore a railway damaged by a great tsunami of the 2011 Great East Japan Earthquake, are reported.

© 2016 Elsevier Ltd. All rights reserved.

### Introduction

Geosynthetic-reinforced soil (GRS) retaining wall (RW) having staged-constructed full-height rigid (FHR) facing (Fig. 1) was developed in the mid-1980s (Tatsuoka et al., 1997a). By extending this GRS RW technology, GRS bridge abutment, placing a girder via a hinged bearing on the top

of FHR facing of a GRS RW, or via a pair of hinged and roller bearings on the top of FHR facings of a pair of GRS RWs, was developed in 1990s (Aoki et al., 2005; Tatsuoka et al., 2005). In 2000s, GRS integral bridge, integrating without using bearings both ends of a continuous girder to the top of the FHR facings of a pair of GRS RW (and also an intermediate pier, or piers if constructed for a long span), was developed (Tatsuoka et al., 2008, 2009, 2012, 2014a,b, 2015). GRS integral bridge is now becoming one of the standard bridge types for railways in Japan (RTRI,

\* Corresponding author. Tel.: +81 471 24 1501; fax: +81 471 23 9766.

E-mail address: [tatsuoka@sepia.ocn.ne.jp](mailto:tatsuoka@sepia.ocn.ne.jp) (F. Tatsuoka).

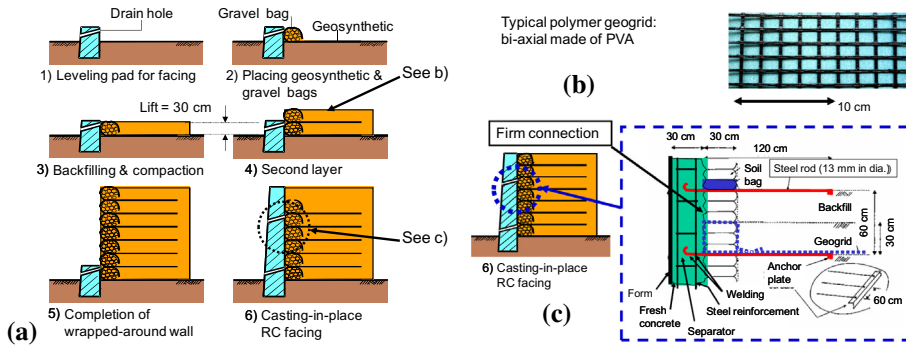
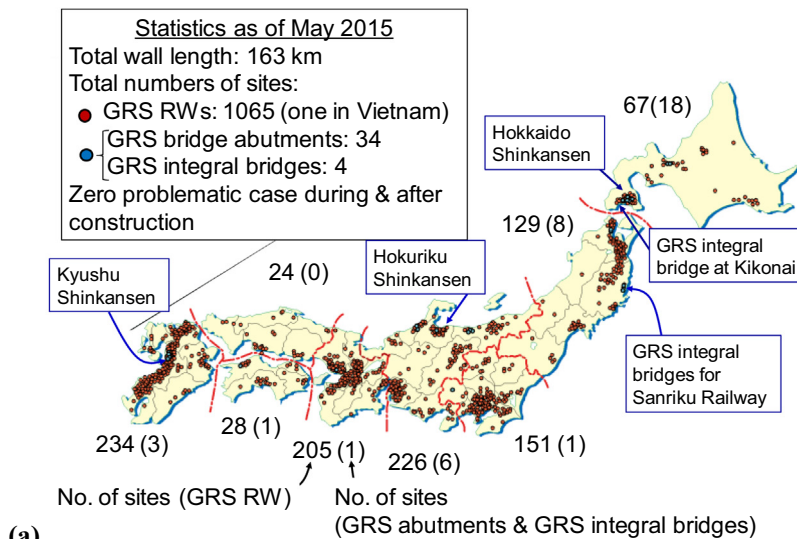
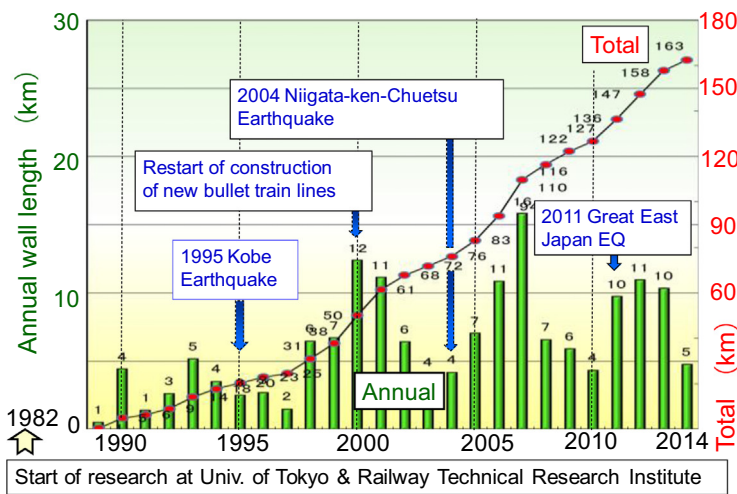


Fig. 1. GRS RW with FHR facing: (a) staged construction; (b) a typical geogrid type; and (c) details of facing construction at stage 6.



(a)



(b)

Fig. 2. (a) Construction sites; and (b) history of GRS structures including RWs with a staged-constructed FHR facing, GRS abutments and GRS integral bridges (as of May 2015).

2012). These types of GRS structure have been constructed at more than 1100 sites (Fig. 2a) and for a total wall length of more than 160 km (Fig. 2b), mainly for railways including high-speed train lines (Shinkansen in Japanese). Many of them were constructed in place of gentle-sloped embankments, cantilever RC RWs, conventional type bridge abutments, RC viaducts and conventional type bridges.

One of the most typical recent cases of GRS structure is the construction of Hokkaido Shinkansen (see Fig. 2a for its location). As described in details by Yonezawa et al. (2014), at many sites within a length of 37.6 km between Kikonai and Shin Hakodate-Hokuto Stations, the following various types of GRS structure were constructed (Table 1). Fig. 3a shows a series of GRS structures constructed at Mantaro section.

- (1) GRS RWs having FHR facing (denoted by R in Fig. 3a) for a total length of 3.5 km: The largest wall height is 11 m. No conventional type cantilever RW was constructed.
- (2) In total 29 GRS bridge abutments (denoted by A in Fig. 3a): The tallest one is 13.4 m-high (Fig. 3b). No conventional type bridge abutment was constructed.
- (3) A GRS integral bridge at Kikonai: This is the first prototype.
- (4) Three GRS box culverts accommodating local roads under-passing the railway (denoted by B in Fig. 3a): Each RC box structure is integrated to GRS RWs at both sides. The tallest one is 8.4 m-high.
- (5) Eleven GRS tunnel entrance protections (denoted by T in Fig. 3a): A GRS arch structure stabilizes the slope immediately above the tunnel entrance to protect trains against falling rocks and sliding soil masses. The tallest one is 12.5 m-high.

The primary reason for such a popular use of GRS structures as described above is high cost-effectiveness together with relatively short construction period and high performance. Among the GRS structures that have been constructed so far (Fig. 2), any problem has not taken place during construction and long-term service and also by prolonged/heavy rainfalls and severe earthquakes despite a wide variety of topological, geotechnical, structural and loading conditions. Despite high performance, the life cycle cost (i.e., the total cost for the construction and maintenance for a full life span) of these GRS structures is much

**Table 1**

GRS structures constructed between Kikonai and Shin Hakodate-Hokuto Stations of Hokkaido Shinkansen (Yonezawa et al., 2014).

| Symbol | Structure type                          | Total length or total number of site | Maximum height (m) |
|--------|---|--------------------------------------|--------------------|
| R      | GRS retaining wall with FHR facing (RW) | 3528 m                               | 11.0               |
| A      | GRS bridge abutment                     | 29                                   | 13.4               |
| I      | GRS integral bridge                     | 1                                    | 6.1                |
| B      | RC box culvert integrated to GRS RW     | 3                                    | 8.4                |
| T      | GRS tunnel entrance protection          | 11                                   | 12.5               |

lower than conventional type soil structures (i.e., gentle-sloped embankments, conventional cantilever RWs and bridge abutments retaining unreinforced backfill). The above is the case in particular when piles become necessary with conventional type soil structures. The following is the important factors for the high cost-effectiveness of GRS structures described above:

- (1) At sites where on-site backfill material is available, embankment retained by this type of GRS RW at both sides is much less costly and more environment-friendly than RC viaducts.
- (2) Ballast-less RC slab track was introduced for Sanyo Shinkansen in 1970s to substantially reduce the maintenance work. Their use was initially limited to tracks on RC structures (i.e., bridges and viaducts). For the southern part (between Tokyo and Nagano) of Hokuriku Shinkansen (opened 1997a) and subsequent Shinkansen lines, RC slab tracks were constructed also on GRS structures. It has been confirmed that the long-term residual settlement of RC slab tracks on GRS structures are negligible (Tatsuoka et al., 2014a,b). The maintenance cost for RC slab tracks is substantially lower than the one for ballast tracks under otherwise the same condition. So, the maintenance cost of GRS structures supporting RC slab tracks is much lower, by a factor of about 0.5, than the one conventional type embankments supporting ballast tracks. For this reason, embankment retained by this type of GRS RW at both sides supporting RC slab tracks is much less costly than gentle-sloped embankments supporting ballast tracks, particularly at sites where the land price is high (Tatsuoka et al., 2014b).
- (3) With an integral bridge, any settlement and lateral displacement at the top of the facing, to which the girder is integrated, that results in structural and functional problems is not allowed. So, it is irrelevant to use any flexible or deformable facing type. If a RC abutment structure is supported with a pile foundation with pure frictional connections to the approach embankment, it becomes difficult to prevent the development of bump due to the settlement of the approach embankment relative to the FHR facing. On the other hand, GRS bridge abutments and GRS integral bridges exhibit negligible bumps by long-term train loads and seismic loads immediately behind the facing. This can be attributed to such staged construction that, after the settlement of the approach embankment associated with its construction has taken place sufficiently, the FHR facing is constructed firmly connecting the geogrid layers reinforcing the approach embankment to the back of the FHR facing.
- (4) During the 1995 Great Kobe Earthquake, gentle-sloped embankments, conventional type RWs, other types of mechanically stabilized earth RW than GRS RWs of this type (Fig. 1), RC viaducts and conventional type bridge abutments were seriously damaged or fully collapsed at many places. In comparison, several GRS RWs of this type all



**Fig. 3.** (a) A view of a variety of GRS structures at Mantaro section of the south part of Hokkaido Shinkansen; and (b) GRS bridge abutment (13.4 m-high) during and after construction, near Mantaro tunnel.

performed very well (Tatsuoka et al., 1997a,b, 1998). A number of GRS RW with FHR facing that had been constructed in the affected areas of the 2011 Great East Japan Earthquake all performed very well without exhibiting any damage requiring for repair works, compared with serious damage or full collapse of other types of soil structures at many places (Tatsuoka et al., 1998, 2014a–c; Kuwano et al., 2012, 2014). They reported a number of discrete panel facings and thin-metal accordion-shaped facings of mechanically reinforced earth RWs using metallic reinforcement elements and flexible type facings of GRS RWs that exhibited large deformation by seismic loading. These experiences have re-confirmed that the seismic stability, as well as the long-term static stability, of this type of GRS RW is very high.

There are several other GRS bridge types that support a simple supported girder on the crest of the reinforced backfill or modular block facing of GRS RW, with or without using a pair of shoes (roller and hinged) (e.g., Zornberg et al., 2001; Abu-Hejleh et al., 2002; Helwany et al., 2003; Lee and Wu, 2004; Skinner and Rowe, 2005; Horvath, 2005). On the other hand, the GRS integral bridge reported in this paper structurally integrates both ends of a continuous girder, not using any bearing, to the top of a pair of FHR facings that are integrated to the geosynthetic-reinforced approach embankment by firmly connecting the geosynthetic reinforcement to the back of the facing. To the best of the authors' knowledge, there is no such full-scale bridge as described above other than those reported in this paper.

### Characteristic features of GRS RW with FHR facing

The characteristic features of the GRS RW system (Fig. 1), which are the basis for the development of GRS integral bridge, are summarized below.

#### Structural features

Tatsuoka (1992) discussed this issue in details. That is, reinforced soil RWs should be stable against both “global

failure along any global failure plane” and “local failure of backfill and facing”. Among many local failure modes, the local failure in the backfill immediately behind the wall face is particularly important. The minimum lateral confining pressure required for this mode of local stability is the active earth pressure with unreinforced backfill. If the wall face is too flexible to develop sufficient earth pressure or if the connection strength between rigid facing and reinforcement is too low, the available earth pressure at the wall face becomes lower than the one required to achieve this type of local stability. Then, the tensile forces in the reinforcement become very low at low levels of the wall, where the active zone between the wall face and the global failure plane starting from the facing bottom is very narrow (Fig. 4a). This results in low confining pressure thus low stiffness/strength in the active zone. This situation may lead to large wall deformation if the backfill is not reinforced very dense. Typical cases of wrapped-around GRS RWs which deformed largely by effects of heavy rain are reported in Tatsuoka and Yamauchi (1986), Tatsuoka (1992), Tatsuoka et al. (1997a, 2000), while those of GRS RWs having flexible facing and metallic-reinforced earth RWs having discrete panel facing or flexible metallic facing that deformed largely by effects of seismic load are reported in Tatsuoka (1992), Tatsuoka et al. (1997b) and Kuwano et al. (2014). With this type of GRS RW having FHR facing with high connection strength (Fig. 1), on the other hand, the available earth pressure at the back of the facing is high enough, thus the tensile forces in the reinforcement can become high enough even at low levels of the wall where the active zone is narrow (Fig. 4b). This results in high confining pressure thus high stiffness/strength in the active zone, preventing the local failure in the backfill, which makes the active zone strong and stiff enough. Then, a high global stability with small wall deformation is not hindered by local failure.

A conventional type RW is a cantilever structure that resists earth pressure. Therefore, large internal force is mobilized in the facing while large overturning moment and lateral thrust force develops at the facing base. Then, a massive facing structure supported by piles usually becomes necessary. These disadvantages become more

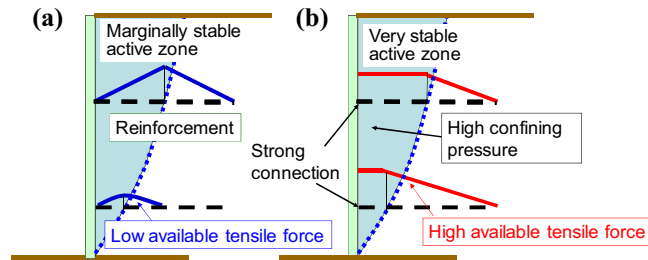


Fig. 4. Available reinforcement tensile forces when the connection strength is: (a) zero; and (b) high (Tatsuoka, 1992).

serious at an increasing rate with an increase in the wall height. On the other hand, the FHR facing of this GRS RW (Fig. 1) is a continuous beam supported by many geogrid layers with a small vertical spacing (i.e., 30 cm). Therefore, only small force is mobilised in the facing even by high earth pressure. Hence, the facing becomes thinner and the structure becomes much simpler using a much less amount of steel reinforcement than cantilever RC RWs retaining unreinforced backfill. Besides, as only small resistance against overturning moment and lateral thrust force at the facing base is required to maintain the global wall stability, piles are usually not used.

When large vertical and/or lateral concentrated load is applied to the top of the facing or on the crest of the backfill immediately behind the facing, high integrity of the active zone is particularly required to maintain high local and global stabilities of the wall. This requirement is satisfied by using a FHR facing to which the reinforcement layers are firmly connected. That is, concentrated load is transmitted to the whole of the FHR facing, then to all reinforcement layers from the top to the bottom of the wall, thereby the concentrated load is resisted by the whole of the wall. Therefore, FHR facing is often used as the foundation for electric poles or noise barrier walls or protective barriers to be constructed on the wall. GRS bridge abutment and GRS integral bridge fully take advantage of these structural features of FHR facing. On the other hand, with reinforced soil RWs having a facing comprising discrete panels or modular blocks, concentrated lateral load applied to the top of the facing or the backfill crest immediately behind the facing is resisted only by the top reinforcement layer or layers connected to a single panel or block at the top, or a couple of top panels or blocks at best. Besides, the facing comprising of discrete panels or modular block cannot support large vertical concentrated load. Tatsuoka et al. (1989), Tatsuoka (1992) and Thamm et al. (1990, 1991) reported typical model tests in which reinforced soil RWs having flexible or deformable facing collapsed due to local failure near the wall face below the crest by vertical concentrated loading on the crest. Although failure of this mode may be somehow alleviated by densely reinforcing the backfill, it is likely that it is very difficult to be stable against outward lateral concentrated loading on the crest.

In addition, with facing comprising discrete panels, the flowable very dry or nearly saturated backfill may flow out through joints between panels if sealing is lacking or insufficient. The GRS RW with FHR facing is free from this type of problem, as the FHR facing has no joints except for

vertical construction joints usually arranged at an interval of 10 m. Moreover, with facing of discrete panels or modular blocks, local failure of a single, or a couple of panels or blocks, which may be associated with local connection failure or local scouring in the subsoil below the facing base, may become collapse of the whole wall. This type of progressive failure is unlikely to take place with the GRS RW with FHR facing, unless most of the connections fail simultaneously or global scouring takes place in the subsoil below the whole facing base, both being usually very unlikely.

#### Staged construction of FHR facing

After potential deformation of subsoil and backfill by the weight of the backfill has taken place sufficiently at construction stage 5 (Fig. 1a), construction stage 6 starts. At stage 6, where FHR facing is constructed by casting-in-place concrete in the space between the geogrid-wrapped-around wall face and the concrete form temporarily supported with steel rods anchored in the backfill (Fig. 1c). In this way, the connection between the facing and the reinforcement layers of geogrid is not damaged by differential settlement between them that may take place if the FHR facing is constructed prior to, or simultaneously with, the construction of the backfill. This procedure is particularly important with GRS bridge abutments and GRS integral bridges, as these structures need a particularly high connection strength between the facing and the reinforcement layers. In the design, the required connection strength is determined by the limit equilibrium analysis taking into account design seismic loads (Tatsuoka et al., 2010a; RTRI, 2012; Yazaki et al., 2013). Besides, with conventional RC RWs, concrete forms and their propping are necessary on both sides of the facing and they become more costly occupying wider space in front of the wall at an increasing rate with an increase in the wall height. With this type of GRS RW, on the other hand, only the outside concrete form anchored in the backfill is necessary, thus only limited space in front of the wall is occupied.

Fresh concrete enters the inside of the gravel-filled bags through the aperture of the geogrid reinforcement wrapping-around gravel bags and the geogrid constituting the bags (Fig. 1c). Then, the facing is eventually firmly connected to the reinforcement layers. As the front end of the geogrid reinforcement is buried in fresh concrete of the facing, the geogrid should have very high resistance against high alkali environment and high adhesiveness

with concrete. So, bi-axial geogrid made of polyvinyl alcohol (PVA) fibre covered with a protection of polyvinyl chloride (PVC) (Fig. 1b) is usually used.

With help of gravel bags placed at the shoulder of each soil layer, the backfill immediately behind the wall face can be compacted efficiently. Prior to the construction of FHR facing, the gravel bags function as a temporary but stable facing unit resisting against earth pressure generated by backfill compaction and the weight of overlying backfill. With completed GRS RWs, the gravel bags function as not only a drain but also a buffer protecting the facing/geogrid connection against potential relative displacements between them by providing an additional strength component to the connection. In the cold regions, such as Hokkaido in Japan, the gravel bags function also as frost heaving restraint.

The design and construction procedures of this type of GRS RW are explained in details in other literatures (e.g., Tatsuoka et al., 1997a, 1998, 2010a, 2014a–c; RTRI, 2012).

### GRS bridge abutment

With conventional type bridges, intolerable bumps often develop immediately behind abutments by depression of unreinforced backfill gradually during long-term service and suddenly by seismic loads. The bump becomes larger by displacements of the abutment and/or the wing RWs. The other problems include needs for a massive RC abutment structure usually supported by piles to restrain the settlement and lateral displacement and to ensure sufficient stability particularly against seismic loads and scouring. To alleviate these problems, a new type bridge abutment, called GRS bridge abutment, was developed (Fig. 5) (Aoki et al., 2005; Tatsuoka et al., 2005). That is, one end of the girder is placed via a hinged bearing on the top of the FHR facing of a GRS RW, or both ends of the girder are placed via a pair of hinged and roller bearings on the top of the FHR facings of a pair of GRS RWs.

For railways, to ensure essentially no bump and a high stability, the zone of the approach embankment immediately behind the facing is usually constructed by well-compacting lightly cement-mixed well-graded gravelly soil that is reinforced with geogrid layers connected to the facing (Fig. 5). As the thickness of the backside uncemented zone behind the cement-mixed zone increases

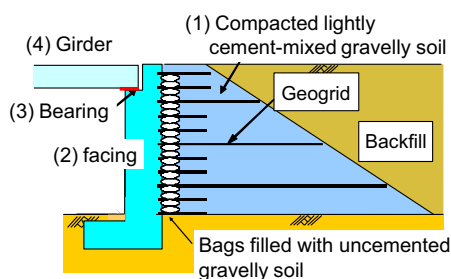


Fig. 5. GRS bridge abutment (the numbers denote the construction steps).

gradually, a bump does not develop at the boundary on the crest between the cement-mixed and uncemented zones even if the uncemented zone exhibits noticeable settlement.

GRS abutment exhibits much higher long-term and seismic stabilities than the conventional type abutment, while it is much less costly due to much more slender RC facing and usually no use of piles. The design and construction procedures of this type of GRS bridge abutment are explained in details in other literatures (e.g., Tatsuoka et al., 2005, 2014b; RTRI, 2012; Tatsuoka and Watanabe, 2015). The first GRS abutment was completed in 2003 for Kyushu Shinkansen (see Fig. 2a for the location). For Hokkaido Shinkansen, in total 29 GRS abutments were constructed fully in place of conventional type abutments (Fig. 3). Until today, GRS abutments for railways were constructed at about 40 sites.

### GRS integral bridge

GRS bridge abutment still has two major serious problems in common with the conventional type bridge: (1) high construction and maintenance cost for bearings; and (2) a low seismic stability of the girder at the bearing against seismic loads. To alleviate these problems, GRS integral bridge (Fig. 6) was developed by extending the technology of GRS bridge abutment (Tatsuoka et al., 2008, 2009, 2012, 2014a,b, 2015). The construction follows steps Nos. 1 through 4 shown in Fig. 6a. That is, after the FHR facing is constructed at stage 3, at stage 4, the continuous girder is constructed with both ends structurally integrated to the top of the FHR facing of a pair of GRS RWs. When the girder is long, say longer than 30 m, a central pier is constructed and the continuous girder is supported only vertically at the top of the pier (Fig. 6c).

GRS integral bridge is more cost-effective exhibiting higher performance than a bridge comprising a simple girder supported by a pair of GRS bridge abutments by the following factors. Firstly, the construction and maintenance of the bearings becomes unnecessary. Secondly, the girder becomes shorter than the simple-supported girder for the same span length. Besides, the girder becomes more slender due to a significant reduction of the maximum bending moment at the center of the girder (by a factor of about 0.5 in the maximum) resulting from flexural resistance at the girder/facing connections. Thirdly, the seismic stability increases significantly due to increased structural integrity and a reduction in the inertial force of the girder due to a decrease in the mass. The stability against tsunami also increases substantially due to increased structural integrity and a reduction in the thrust tsunami load on the girder due to a decrease in the thickness. It is to be noted that the importance of high resistance against tsunami was recognized after vast damage to a great number of conventional simple-supported girder bridges during the 2011 Great East Japan Earthquake, as described later in this paper.

As the GRS integral bridge is a highly in-deterministic structure, settlement of facing by, for example, compression of soft ground or scouring that results into structural

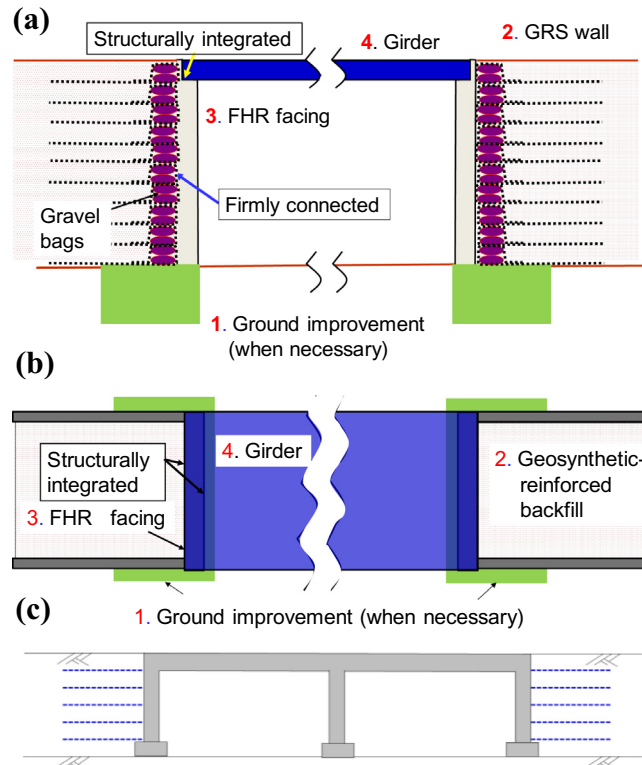


**Fig. 6.** Structure of GRS integral bridge (the numbers denote the construction steps): (a) elevation; (b) plan; and (c) a long span bridge with the girder supported by a central pier.

and functional damage to the bridge is not allowed. In this respect, if the FHR facing supported by a pile foundation is constructed before the construction of the approach embankment, the approach embankment settles down relative to the facing developing a bump back of the facing. With the GRS integral bridge, the FHR facing is constructed after the ground settlement by the weight of the approach embankment has taken place sufficiently. Therefore, even without being supported by pile foundations, the facing becomes free from settlement by the weight of approach embankment while the problem of bump does not take place. Yet, relevant ground improvement of soft soil layers if they exist in the supporting ground becomes necessary to ensure negligible residual settlements of the facing during a long service period. The construction of a GRS integral bridge on a thick soft soil deposit or ground susceptible to deep scouring is one of the current technical issues to be solved.

#### Model tests

The GRS integral bridge was developed based on a series of model shaking table tests in the laboratory and analysis of the test results (Tatsuoka et al., 2008, 2009, 2012; Munoz et al., 2012), followed by the construction of a full-scale model (Fig. 7a and b; Nagatani et al., 2009) and full-scale loading tests performed three years after its construction (Fig. 7c: Suga et al., 2012; Koda et al., 2013). As described below, the stability of the full-scale model was

evaluated by applying cyclic lateral loads simulating thermal deformation of the girder and level 2 design seismic load to the girder of the model. The current seismic design method of GRS integral bridge is described in Yazaki et al. (2013).

The full-scale model of GRS integral bridge (Fig. 7a) simulating a single-track railway bridge comprises a 3.0 m-wide and 14.75 m-long continuous girder, a pair of 5.55 m-high FHR facings and a pair of approach embankments. This model was constructed spanning a pair of full models of GRS RW having FHR facing constructed in a period from the beginning of 1997–1998 (Tatsuoka et al., 1997a, 2000). A pair of approach blocks of the abutments were constructed by excavating the backfill of these two full-scale models of GRS RW. As seen from Fig. 7b, both lateral sides of the respective approach blocks are in contact with the sheet piles retaining the backfill of the existing GRS RW via a lubricated interface comprising a grease layer sandwiched by plywood sheets arranged to minimize the shear stresses on the lateral faces of the approach fill during the full-scale loading tests described below. Table 2 lists the construction materials and structural dimensions.

Two types of approach block that are currently used for railways in Japan were constructed by compacting either well-graded gravelly soil (GS) (crushed hard rock from a quarry, M-40) or cement-mixed M-40 with a dry weight ratio of cement to gravel equal to 4%. The compressive strength of compacted cement-mixed gravel was designed to be at least 2 MPa at a curing period of 28 days. Approach

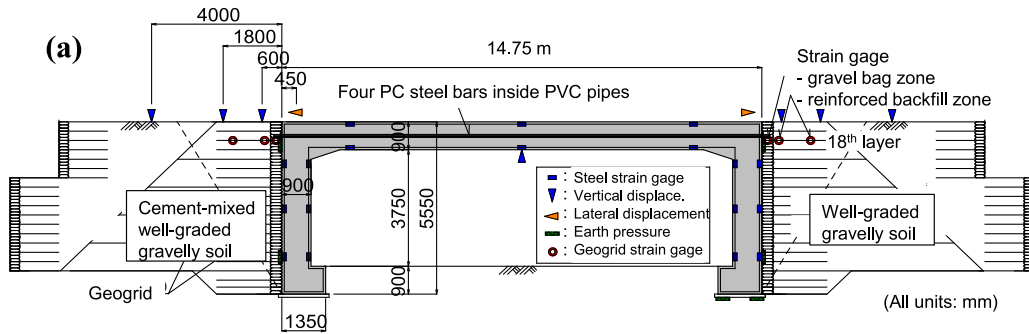


Fig. 7. A full-scale model of GRS integral bridge constructed at Railway Technical Research Institute: (a) overall structure (Suga et al., 2012); (b) the left side abutment in Fig. a under construction (27 November 2008); and (c) full-scale loading test (January 2012) (Koda et al., 2013).

blocks of compacted gravelly soil are used for ordinary train lines. On the other hand, well compacted cement-mixed GS is used mainly for high speed train lines (Shinkansen) to minimize the amount of bump that may develop immediately behind the RC abutment, as

explained above related to Fig. 5. With GRS integral bridges, an increase in the seismic stability of whole bridge system is the other purpose of using cement-mixed GS approach block (Tatsuoka et al., 2009). With both types of approach block of the full-scale model (Fig. 7a), the

**Table 2**

Construction materials and structural dimensions of full-scale GRS integral model (Koda et al., 2013).

|  |                                   |  |
|--|-----------------------------------|--|
| Bridge dimensions                      | Girder length                     | 14.75 m                                  |
|  | Width                             | 3 m                                      |
|  | Girder thickness                  | 0.9 m                                    |
|  | Facing thickness                  | 0.9 m                                    |
|  | Foundation                        | Spread footing                           |
| Concrete                               | Cement                            | Ordinary portland                        |
|  | Design compressive strength       | $f_{ck} = 27 \text{ N/mm}^2$             |
| Steel reinforcement                    | Type                              | SD345                                    |
|  | Main reinforcement                | D19ctc150 mm (footing & facings)         |
|  |                                   | D22ctc150 mm (girder)                    |
| Geogrid                                | PVA fiber covered with PVC        | Design tensile rupture strength          |
| Approach fill                          | Well-graded gravelly soil (WG GS) | $T_a = 60 \text{ kN/m}$                  |
|  | Cement-mixed WG GS                | M-40                                     |
| Backfill in back of the approach block |                                   | M-40 mixed with ordinary Portland cement |
|  |                                   | C-40 (crusher run)                       |

backfill was reinforced with 19 layers of geogrid with a vertical spacing of 30 cm. The geogrid has a bi-axial structure comprising PVA fibre covered with a protection of PVC, thus it has a very high resistance against high alkaline. This feature is one of the most important features required for the geogrid to be used for GRS integral bridges, as the end part of the geogrid is buried in a concrete layer of the facing for a firm connection. With this type of geogrid, the allowable tensile strength  $T_a$  is reduced by a factor of 0.8 from the yield tensile strength based on a minimum average role value, while the design long-term tensile strength is typically 0.6 times  $T_a$  and the seismic design value against realistic high seismic load is 0.9 times  $T_a$  (RTRI, 2012).

Three layers of gravel-filled geogrid bags with a compacted thickness of about 10 cm per each and a compacted width of about 40 cm were placed at the shoulder of each soil layer between the vertically adjacent geogrid layers (Fig. 7b). With help of these gravel-filled geogrid bags, the backfill was compacted so that the compacted thickness of respective soil layers became 15 cm and the degree of compaction (i.e., the ratio of compacted dry density to the maximum dry density by the modified Proctor) became at least 95%. With the approach block of cement-mixed gravel approach block, 40 cm-wide unbound gravel-filled geogrid bags immediately behind the FHR facing should absorb cyclic displacements caused by seasonal thermal deformation of the girder. As described later in this paper, these unbound gravel zone was made wider for the two GRS integral bridges having longer girders (40 m and 60 m) for Sanriku railway.

Table 3 shows the outline of two types of full-scale cyclic lateral loading tests that were performed simulating lateral cyclic loads in the bridge axis direction due to (1) thermal expansion and contraction of the girder; and (2) L2 level design seismic load, which is as severe as the highest horizontal acceleration recorded on the ground during the 1995 Great Kobe Earthquake. Lateral loads were applied to the girder by using four hydraulic jacks with a capacity of 1000 kN/each on each side (so in total eight jacks). A set of four jacks were fixed to a steel reaction frame arranged at each end of the model (Fig. 7c). The tensile load from the jacks was transmitted to steel rods in sheaths buried in the approach blocks on both sides of the model, which

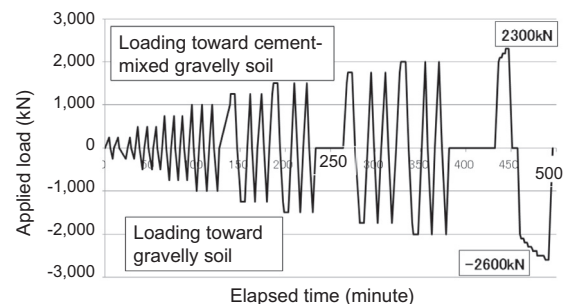
was then transmitted to four PC steel bars arranged in PVC pipe sheaths buried in the girder. Both ends of the PC steel bars were fixed to the end faces of the girder by using steel plates and bolts so that the tensile loads from the jacks were fully transmitted as compressive loads to the respective ends of the girder. The peak lateral load was set equal to 500 kN to simulate an expansion/contraction of the 15 m-long girder by a change in the temperature equal to 20 °C. 50 cycles were applied simulating a period of 50 years (i.e., the design life time). It has been confirmed that effects of daily changes in the temperatures are negligible when compared with those of annual changes (Hirakawa et al., 2006, 2007; Tatsuoka et al., 2010a).

Subsequently, 50 cycles with a peak load of 1000 kN were applied to examine the behavior by more severe,

**Table 3**

Two series of lateral cyclic loading tests (Koda et al., 2013).

| Loading method   | Loading history  | Objective                                    |
|--|--|--|
| One-side cyclic loading ( $H$ : constant single amplitude of lateral load)   | 50 cycles of $H = 500 \text{ kN}$ in two directions; and 50 cycles of $H = 1000 \text{ kN}$ in two directions                      | Simulation of seasonal thermal displacements |
| Reversed cyclic loading with a vertical train load $W_{\max} = 35 \text{ kN/m}$ on the girder ( $H_{\max}$ : largest lateral load) | $H_{\max} = 2300 \text{ kN}$ when loading toward cement-mixed GS<br>$H_{\max} = 2600 \text{ kN}$ when loading toward gravelly soil | Simulation of Level 2 design seismic load    |

**Fig. 8.** Reversed cyclic loading simulating seismic loads.

exceptional temperature effects simulating an annual temperature change equal to 40 °C.

Fig. 8 shows the time history of reversed cyclic loads applied to evaluate the behavior of the GRS integral model when subjected to seismic loads up to L2 level design seismic load. A series of three symmetric reversed cyclic loads were applied stepwise increasing the single amplitude from 250 kN to 2000 kN. In the last cycle, a maximum lateral compressive load equal to 2300 kN was applied toward the cement mixed gravelly soil approach block, followed by a maximum load equal to 2600 kN toward the well-grade unbound gravelly soil approach block. A lateral load of 2200 kN is equivalent to the inertial of the girder by a peak response acceleration equal to 1.0 g (i.e., the gravitational acceleration).

In the model shaking table tests performed in the laboratory (Tatsuoka et al., 2009; Munoz et al., 2012), the failure of the GRS integral bridge model started with the passive failure at the top part of the approach fill of the abutment on the passive side caused by the lateral inertia load of the girder. Therefore, the evaluation of this factor is indispensable in the seismic design of GRS integral bridge. In this respect, under actual seismic loading conditions, as well as in the model shaking table tests, not only the girder but also the abutments comprising the facings and the approach fills on both sides exhibit seismic response accelerations, which are usually lower than the response acceleration at the girder. Therefore, unlike this full-scale pseudo-static cyclic loading test, the inertia of the girder is not fully activated as the lateral push-in load to the abutment on the passive side (Factor A). At the same time, this lateral load by the inertial of the girder is reduced by the tensile resistance of the geogrids layers attached to the facing of the abutment on the active side. This tensile resistance under actual seismic loading conditions should be much smaller than the one in these full-scale loading tests, in which the seismic inertia of the abutment on the active side is zero (Factor B). The shaking table model tests showed that the effect of Factor B is smaller than that of Factor A. Therefore, the lateral push-in load to the abutment on the passive side and associated damage to the facing and approach fill of the abutment on the passive side under actual seismic loading conditions should be smaller than the one for the same inertial load applied in this full-scale loading test. For the same reason, the lateral displacements of the girder relative to the abutments under the actual seismic condition should be much smaller than those for the same inertia of the girder observed in this full-scale test. This conservative simplification of seismic loading employed in this full-scale pseudo-static cyclic loading test is adopted when evaluating the damage to the facings, approach fills and geogrid layers in the current seismic design of GRS integral bridge (Yazaki et al., 2013).

The essence of the results from the reversed lateral cyclic loading test simulating seismic loading is herein described. Figs. 9a and b show the relationships between the lateral load and the lateral displacements at the top of the facing on both sides of the model. Figs. 10a and b show the envelopes of the relationships presented in Figs. 9a and b. It may be seen from these figures that, when the peak lateral load was lower than about 1000 kN, the

behaviour is highly reversible, showing that the damage to the approach blocks (including the facing, gravel bag zone and geogrid-facing connection) was very small. This result is consistent with the highly reversible behaviour observed in the cyclic loading test simulating thermal effects with a peak lateral load of 1000 kN.

As the peak load exceeded about 1000 kN, the load–displacement relation started exhibiting hysteresis relations with noticeable areas and this trend became more obvious with an increase in the peak load. In the last cycle, in which the peak load exceeded the L2 design seismic load, the residual displacements at both sides became particularly large, probably due mainly to yielding of the geogrid immediately behind the connection at the back face of the facing, where nearly full pull-out load is applied to the geogrid while the tensile forces in the geogrid at deeper places embedded in the backfill became lower. Yet, the peak displacement at the top of the facings in the active and passive modes when the applied lateral load became the L2 seismic load was only about 20 mm on both sides. This very high performance can be attributed to such features of GRS integral bridge that all the major structural components (i.e., a girder, a pair of facings and a pair of geosynthetic-reinforced approach blocks) are all integrated to each other and they all together resist applied loads. In particular, unlike the conventional type integral bridge (with unreinforced backfill), the resistance by tensile forces in the geogrid layers in the high level part on the active side are activated simultaneously with the resistance by compressive forces in the high level part of the approach block on the passive side. As the secondary component of the resistance, the tensile forces in the geogrid layers at low levels on the passive side and compressive forces in low level part of the approach block on the active side are also activated at the same time to restrain rotational displacements of the FHR facings.

It may also be seen from Fig. 10a and b that the differences between the displacements in the active and passive modes at the respective approach fills and between the two types of approach block are insignificant. It is likely therefore that the displacements when both approach blocks are made of cement-mixed GS are not significantly smaller than that of the stiffer response in Figs. 10a and b, while the displacements at the top of the facing when both approach blocks are made of unbound gravelly soil are not significantly larger than that of the softer response presented in Figs. 10a and b. Yet, it may be seen from Fig. 10a that the displacement in the active mode at the top of the facing for the approach block of cement-mixed GS was noticeably smaller than that for the approach block of unbound gravelly soil. It may also be seen from Fig. 10b that the displacement in the passive mode at the top of the facing for the approach block of unbound gravelly soil was noticeably smaller than that for the approach block of cement-mixed GS. These results show that the displacement of the girder was noticeably smaller when the compressive load was activated toward the unbound gravelly soil approach fill (i.e., the cases with a superscript \* in Figs. 10a and b) than when the compressive load was activated toward the cement-mixed GS. It is likely that these trends are due to the following two

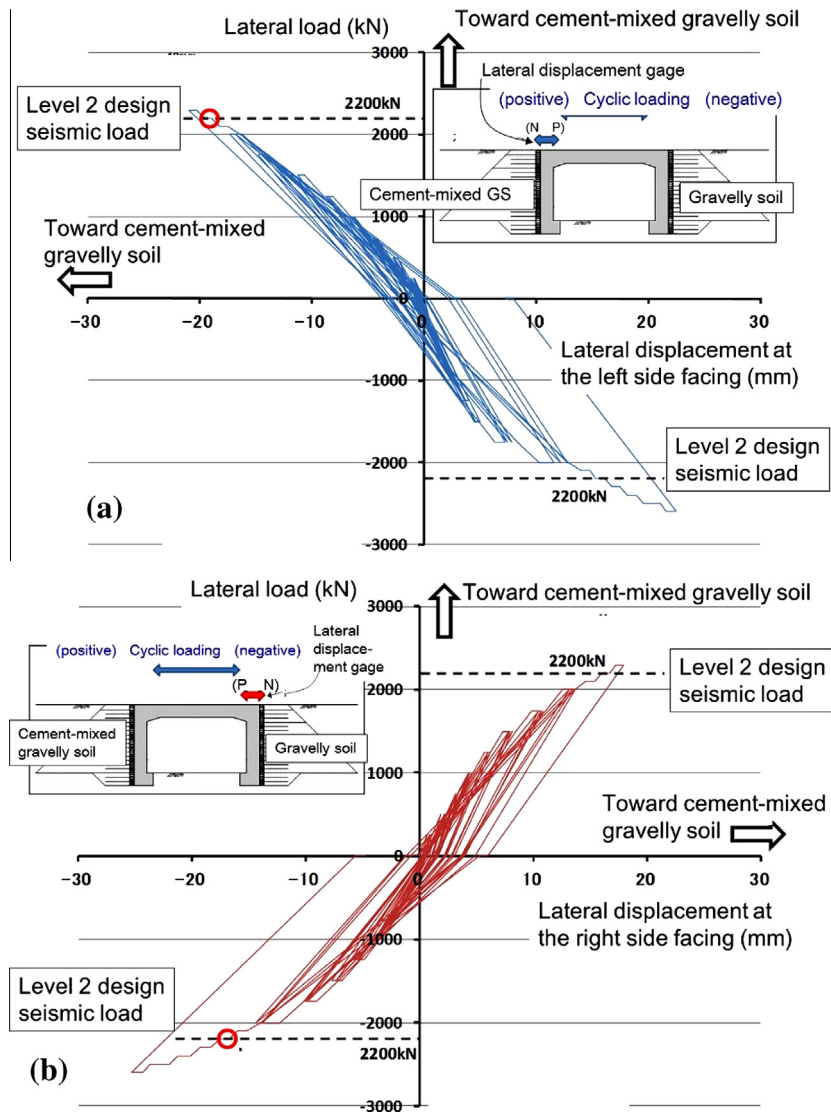


**Fig. 9.** Relationships between the lateral load and the lateral displacement at the top of the facing for: (a) cement-mixed gravelly soil approach block; and (b) gravelly soil approach block, from reversed lateral cyclic loading test (Koda et al., 2013).

factors. Firstly, the tensile stiffness of the geogrid in the approach block of cement-mixed GS is larger than the one in the approach block of unbound gravelly soil. It is likely that the tensile deformation of the geogrid in the approach block of cement-mixed GS is more restrained due to much higher stiffness of cement-mixed GS. Secondly, the coefficient of lateral sub-grade reaction for compression of the approach block of cement-mixed GS is similar as the one of the approach block of unbound gravelly soil. That is, it is likely that the values of compressive stiffness of the approach blocks of cement-mixed GS and of unbound gravelly soil are similar, because both are largely controlled by the compressive stiffness of the unbound gravel-filled bags arranged immediately back of the FHR facings.

In this loading test program, uniform static vertical load of 35 kN/m simulating train loads under design seismic

conditions was applied to the full length of the girder. The vertical settlement at the center of the girder was only 1.4 mm, which is much lower than the allowable serviceability limit (i.e., 19 mm for safe train operation and 6 mm for comfortable riding, both when a train speed is 260 km/h; RTRI, 2012). These serviceability limits are much smaller than the structurally ultimate limit. This result indicates that this full-scale GRS integral bridge will exhibit no problem during ordinary long-term service when used as an actual railway bridge for a high-speed train line.

All the results from the construction of this full-scale GRS integral bridge model and this loading test program confirmed that the GRS integral bridge can be constructed at many places in place of conventional simple-supported girder bridges as much more cost-effective bridges exhibiting higher performance with a reduced construction period and a reduced maintenance cost.

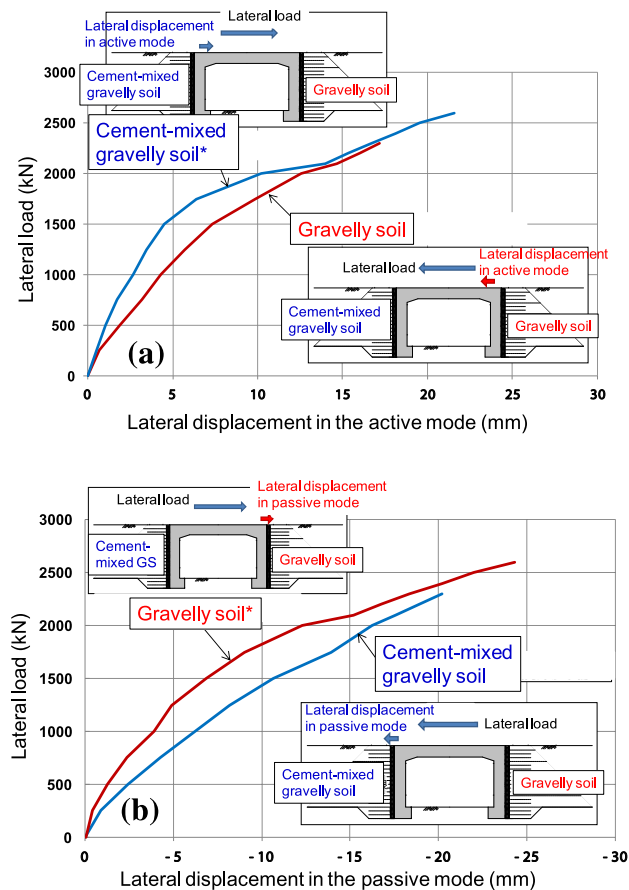


**Fig. 10.** Envelopes of the relationships between the lateral load and the lateral displacements at the top of the facing for displacements in: (a) active mode; and (b) passive mode, from reversed lateral cyclic loading tests (Koda et al., 2013).

The design and construction procedures of GRS integral bridge are explained in details in other literatures (e.g., Tatsuoka et al., 2015; Koda et al., 2013; Yazaki et al., 2013; RTRI, 2012; Tatsuoka and Watanabe, 2015).

#### First GRS integral bridge

The first GRS integral bridge was constructed as an over-road bridge at Kikonai for Hokkaido Shinkansen (Figs. 11a–c; see Fig. 2a for the location). Yonezawa et al. (2014) reported that the construction cost of this bridge was estimated to be about a half of that of the equivalent conventional type simple-supported girder bridge with unreinforced approach embankment. They also reported other factors by which it was decided to adopt this first GRS integral bridge opposed to going with the more standard GRS abutments at the time. To confirm a high stability of this bridge, including the one against thermal deformation of the girder, ambient temperature, strains in the geogrid and steel reinforcement, displacements and earth pressures at selected places were observed from a period during the construction stage. Fig. 11d shows the time histories of ambient temperature and lateral displacements at the top and bottom of the two facings relative to the approach blocks. The locations where these displacements

were measured are indicated in Fig. 11a. Fig. 11e shows the corresponding relationship between the apparent deflection of the girder obtained from these measured displacements and the average temperature inside the girder. The amplitude of the annual lateral displacement change at the top of each facing is about 3 mm, which is about 0.05% of the wall height, 6 m. Thus, the amplitude of the annual thermal girder length change is about 6 mm, which is about 0.05% of the girder length, 12 m. By the thermal expansion of the girder in summer, the top of the facing is pushed towards the approach blocks and the tension force in the geogrid reinforcement decreases. By the thermal compression of the girder in winter, the top of the facing is pull from the approach block and the geogrid tension increases. These responses are negligible at the bottom of the facings. It has been confirmed that the bridge is not over-stressed at all. This high performance can be attributed to that the structural components of the bridge (i.e., the girder, a pair of FHR facing and a pair of approach blocks) are structurally highly integrated.

The peak value of the active displacement relative to the approach block at the top of the facing (i.e., the measured compression of the girder) in the third winter (around January 2014) is slightly larger than the one in the second winter (around January 2013) (Figs. 11d and e).

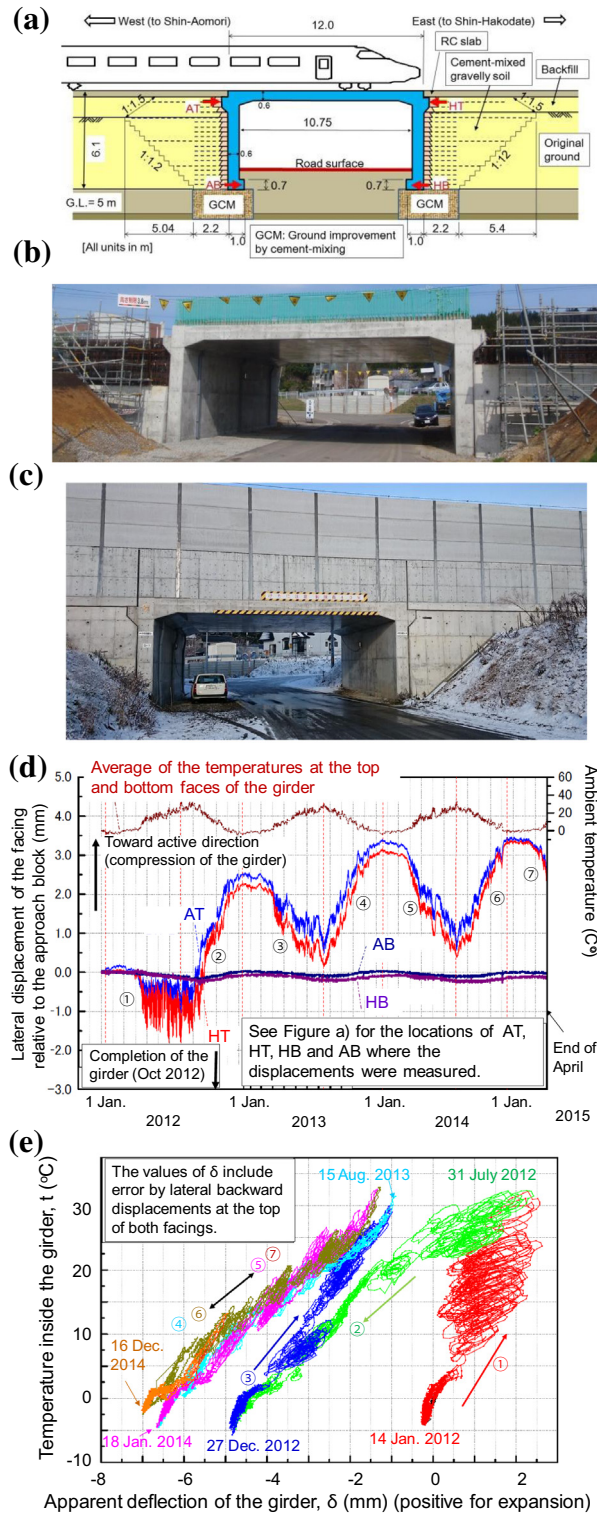


**Fig. 11.** GRS integral bridge at Kikonai: (a) structure; (b) under construction; (c) completed; (d) time histories of ambient temperature and horizontal displacements at the facing by the end of April 2015; and (e) relationship between the apparent deflection of the girder and the average temperature inside the girder during terms 1 through 7 indicated in Fig. d (Sasaki et al., 2014 and additional data).

This phenomenon is due only partly to the drying shrinkage of the concrete of the girder but it is due mainly to a slight lateral backward displacement at the top of both facings (which is the reference points for the measurements of the girder deflection) caused by a slight rotational displacements about the facing bottom in the passive direction of the approach block. This behavior resulted from the delayed compression of the original ground beneath the approach blocks caused by the weight of a thin top backfill layer placed on both approach blocks. Although this backfilling should have been done before the construction of the facing and girder, it was performed at the final construction stage due to a restraint in the construction schedule. The displacement is very small and its effect is negligible. Moreover, as seen from Fig. 11d, the peak active displacements at the top of the facings at the third winter (i.e., around January 2014) and the fourth mid-winters (i.e., around January 2015) are the nearly same. Besides, as seen from Fig. 11e, the relationships between the apparent deflection of the girder and the temperature in the girder observed in the terms denoted by numbers 4 through 7 (from the fall of 2013 to the spring of 2015) overlap each other nearly perfectly. These results indicate that the delayed compression of the ground and backfill has nearly perfectly completed by the third winter (i.e., around January 2014). Yet, this event should be appreciated as an incident from which we should learn a lesson.

### Three GRS integral bridges restoring collapsed bridges

By the 2011 Great East Japan Earthquake, the girders and/or approach fills of more than 340 bridges for roads and railways running near coasts were washed away by a great tsunami. Sanriku Railway, opened 1984, is running along the coastline (see Fig. 2a for the location). Although this railway was constructed at a relatively high elevation based on the previous tsunami disasters in 1896 and 1933, the tsunami this time was much higher than had been anticipated. Typically, the run-up height was 22–23 m at

Shimanokoshi (Fig. 12). In particular, the three sites (Haipe, Koikorobe and Shimanokoshi) shown in Fig. 12 are located in three narrow valleys between tunnels, where the railway track level was lowest (12.3–14.5 m) and the bridges were located closest to the coastal line along the whole of Sanriku Railway. In addition, there was no coastal dyke between the railway and the coastal line. The tunnels were inundated and the damage to the railway structures was very serious. The simple-supported girders of three bridges were washed away. The abutments and piers and their foundations of the bridges were also seriously damaged, while the part above the ground level of many of them was washed away. These collapsed bridges were restored by constructing three GRS integral bridges as cost-effective bridges that are highly tsunami-resistant. The railway was re-opened 6th April 2014, about three years after the earthquake.

### Haipe-sawa GRS integral bridge

The previous bridge at Haipe comprised two simple supported-girders. The girders were fully washed away as shown in Figs. 13a and b. A GRS integral bridge was constructed taking advantage of part of the foundations that survived the great tsunami and were remaining at the original places whereas their upper parts were washed away (Fig. 13c). The total length of a continuous girder of the GRS integral bridge at the site is 60 m, which is much longer than the one at Kikonai (Fig. 11). The width of the girder for a single track is 6.7 m. Both ends of the girder are structurally integrated to the top of the FHR facings of a pair of GRS RWs and a central pier designed to support only the vertical load. Fig. 14a shows the north abutment immediately before constructing a FHR facing. A through girder (Fig. 13d) was employed to ensure a sufficient free height below the girder for a local road under-passing the bridge. A steel-framed steel-reinforced concrete (SRC) structure was adopted to decrease the thermal deflection (i.e., contraction in winter and extension in summer) of this relatively long-span girder. A PC girder was not adopted, because the summation of elastic contraction when introducing pre-stress, creep contraction and drying shrinkage becomes larger by a factor of 20 than the SRC girder, thus a PC girder would exhibit a much larger total contraction in winter. Too large contraction of the girder may extend too much and may damage the geogrid located in the unbound gravel zone immediately behind the facing (Fig. 14b). In addition, prepared for relatively large thermal length changes of this relatively long SRC girder, the width of the unbound gravel zone immediately behind the facing was made 1.0 m, compared with 40 cm of gravel-filled bags employed with shorter GRS integral bridges: i.e., the full-scale model (Fig. 7) and the one at Kikonai (Fig. 11) and the one at Shimanokoshi (Fig. 18 shown later). In so doing with the GRS integral bridges at Haipe-sawa and Koikorobe-sawa, as shown in Fig. 14b, welded metal wire mesh boxes were used in place of geogrid bags. The use of wire mesh boxes is to reduce construction time. The use of gravel bag is preferable by a higher self-adjustable deformability due to a high flexibility if the construction time is not an issue. The acceptable performance of the connection part against relatively large thermal

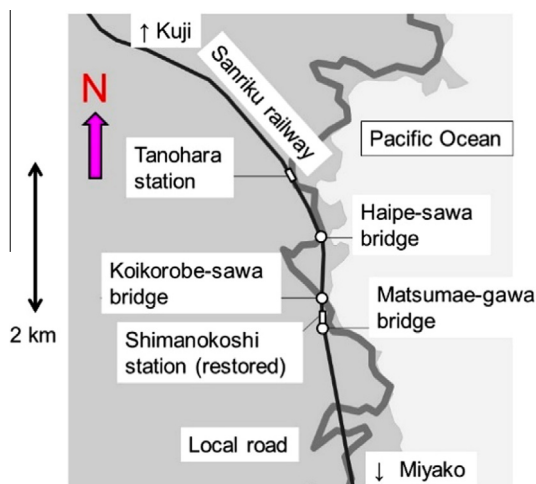
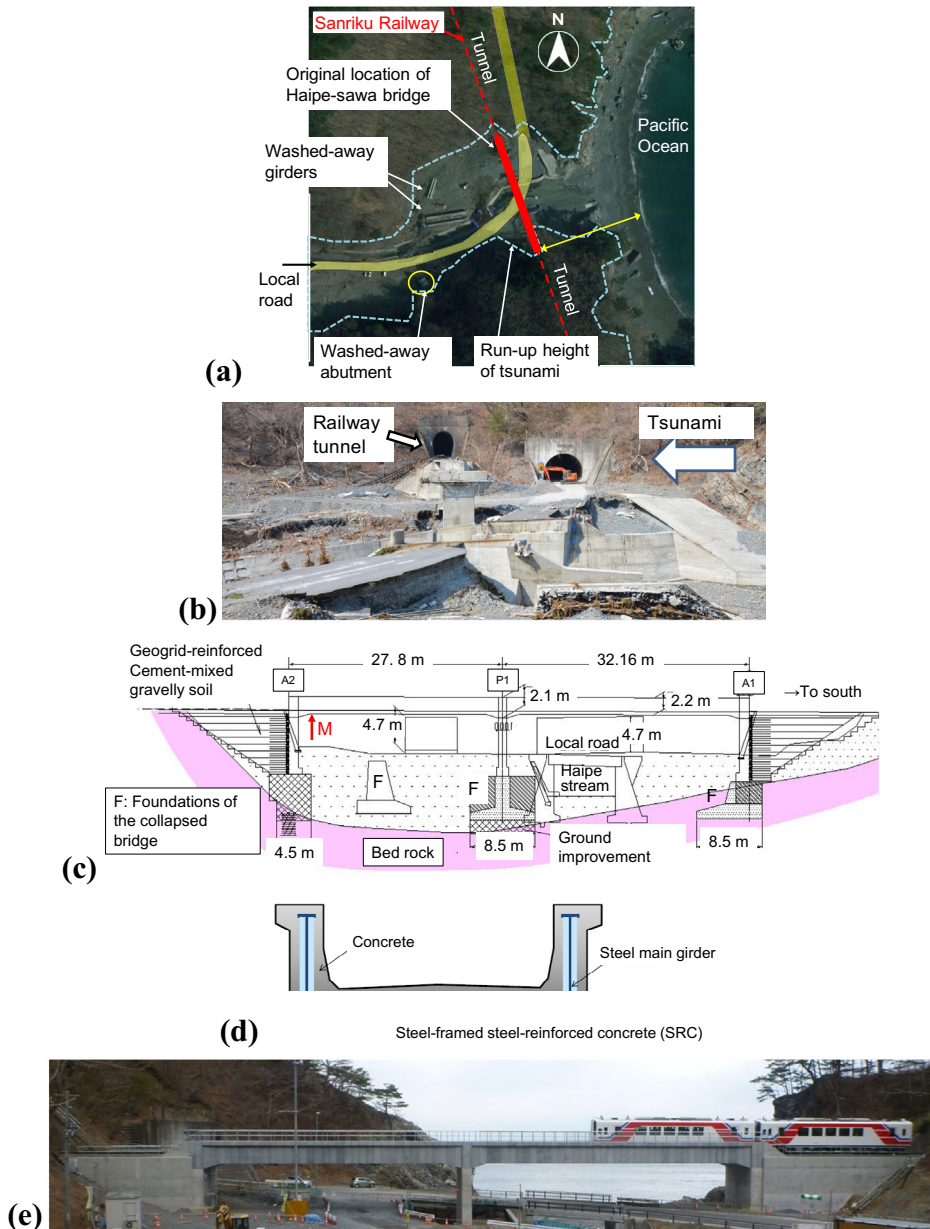


Fig. 12. Locations of Haipe, Koikorobe and Shimanokoshi along Sanriku Railway.



**Fig. 13.** Haipe-sawa bridge, Sanriku Railway: (a) aerial photo immediately after collapse and (b) from south (30 March 2011); (c) structure of GRS integral bridge seen from the inland; (d) typical cross-section of the through girder; and (e) completed GRS integral bridge (6th April 2014).

deformation of the girder and severe design seismic load of level 2 was examined and ensured by performing cyclic loading tests of a full-scale partial model simulating the connection part shown in Fig. 14b (Tamura et al., 2013).

The stability against tsunami of the GRS integral bridge at Haipe-sawa and the one at Koikorobe-sawa (explained below) were evaluated and compared with that of the previous two-span simple-supported girder bridges, which were fully washed away by the great tsunami of the 2011 Great East Japan Earthquake. The stability was evaluated against the estimated maximum tsunami height above the rail level of the actual tsunami, which is 8.2 m

(Koikorobe) and 4.4 m (Haipe) (Shindo et al., 2015). With the two simple-supported girders of the previous bridge at Haipe, the ratio of the tsunami lateral load to the resistance is 5.85 and 5.65 while the ratio of the tsunami uplift load to the resistance is 1.42 and 1.98. With the two simple-supported girders of the previous bridge at Koikorobe, the ratio of the tsunami lateral load to the resistance is 5.32 and 9.92 while the ratio of the tsunami uplift load to the resistance is 3.04 and 2.63. These values significantly higher than unity are consistent with the actual serious damage by tsunami. On the other hand, the GRS integral bridges constructed at Haipe-sawa and Koikorobe-sawa,

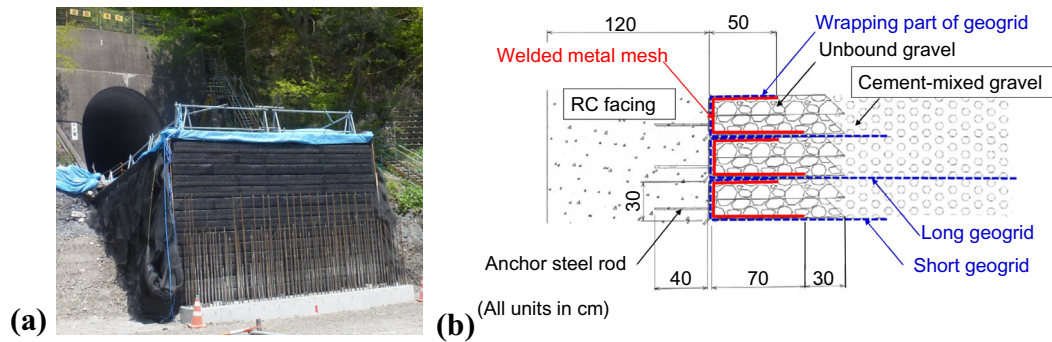


**Fig. 14.** Heipe-sawa GRS integral bridge: (a) a view of the north abutment immediately before constructing FHR facing (22 May 2013); (b) the structure of connection between the RC facing and the geogrid reinforcement.

the evaluated ratio of the tsunami lateral load to the resistance is respectively 1.00 and 0.99, while the ratio of the tsunami uplift load to the resistance is respectively 0.42 and 0.61. These low ratios equal to, or lower than, 1.0 indicate that the GRS integral bridges are substantially more stable against tsunami than the conventional simple-supported girder bridges, while these GRS integral bridges would have survived the actual tsunami if they had been existing at the time of that earthquake. This high stability of GRS integral bridge results from high integrity of the girder, the facings and the approach blocks. Kawabe et al. (2015) reported the results of the small model tests supporting this analysis.

Fig. 15a shows the time histories of ambient temperature and geogrid strains measured at horizontally arranged four points immediately behind the facing at a level near the crest of the wall of the north abutment for a period during construction in the year of 2013. As shown in the figure inset in Fig. 15a, points 6-1 and 6-2 are located in the unbound gravelly soil zone, while points 6-3 and 6-4 are in the cemented gravelly soil zone of the approach block. The geogrid strains at points 6-1 and 6-4 are relatively small due to restraint of, respectively, a welded metal mesh member (used at this site in place of gravel-filled geogrid bags, Fig. 1a) and cement-mixed gravelly soil. Upon the structural integration of the girder to the top of the facings, the geogrid strains at point 6-2 and 6-3 started sensitively responding to ambient temperature changes, similarly as the GRS integral bridge at Kikonai. Fig. 15b shows the relationships between the horizontal displacement at the top of the facing relative to the approach block and the geogrid tensile strain at point 6-2 in both abutments. It may be seen that the instantaneous ratio of geogrid strain increment to active horizontal displacement increment,  $d\varepsilon_g/d\delta$ , decreases once  $\delta$  exceeds the previous maximum value ( $\delta_{\max}$ ), while the  $\varepsilon_g - \delta$  relation becomes rather reversible as far as  $\delta$  is kept smaller than  $\delta_{\max}$ . It may be seen by carefully examining Fig. 15a and b that this trend of behavior is due to the fact that the geogrid strain at point 6-1 increases noticeably only when  $\delta$  exceeds  $\delta_{\max}$ . This is due likely to that the welded metal mesh restrains strongly the geogrid strain at point 6-1 as far as  $\delta$  is smaller than  $\delta_{\max}$ . This trend indicates that the geogrid deforms more uniformly in the

unbound gravelly soil zone once  $\delta$  becomes larger than  $\delta_{\max}$ . This mechanism is preferable as it keeps the maximum geogrid tensile strain smaller than the value when this mechanism is not effective.

Fig. 15c shows the time histories of ambient temperature and the lateral displacements at the top and bottom of both FHR facings,  $\delta$  (positive for active displacements), for a period of about two and a half years starting the moment at the end of the period indicated in Fig. 15a, which is about one month after the integration of the girder to the FHR facings (5th October 2013).  $\delta$  is defined zero at the starting point for the measurements presented in Fig. 15c, which is close to the time when the girder was integrated to the facings. It may be seen from Fig. 15c that the displacements at the bottom of the FHR facings are essentially zero, indicating that the FHR facings are rotating about their bottom. This trend of behavior is the same as the GRS integral bridge at Kikonai (Fig. 11d). The displacements at the top of the two FHR facings are nearly the same and the amplitude at the respective sides is about 6 mm. This result indicates a nearly symmetric thermal deformation of the girder about its center.

The amplitude of the length change of the girder during the initial observation period described in Fig. 15a and b was about 6 mm, while the amplitude during the first full year period was about 12 mm (Fig. 15c). 12 mm is 0.02% of the girder length, 60 m. This amplitude of the thermal strain of the girder is much smaller (by a factor of about 0.4) than the value of the GRS integral bridge at Kikonai, 0.05%. This is due to the use of SRC girder at Haipe, compared with the RC girder at Kikonai. The maximum geogrid tensile strain shown in Fig. 15a is about 0.05%. The maximum strain during the first and second full year periods was larger, about 0.14%, which is still substantially lower than the design allowable value, 3%.

Fig. 15d shows the relationship between the thermal deflection (positive for expansion) of the girder, shown in Fig. 15c, and the temperature measured inside the girder for the period indicated in Fig. 15c. The numbers 1–6 denote the terms indicated in Fig. 15c. The broken line represents the following theoretical relation when the thermal deflection of the girder takes place free from any restraint of the abutments:

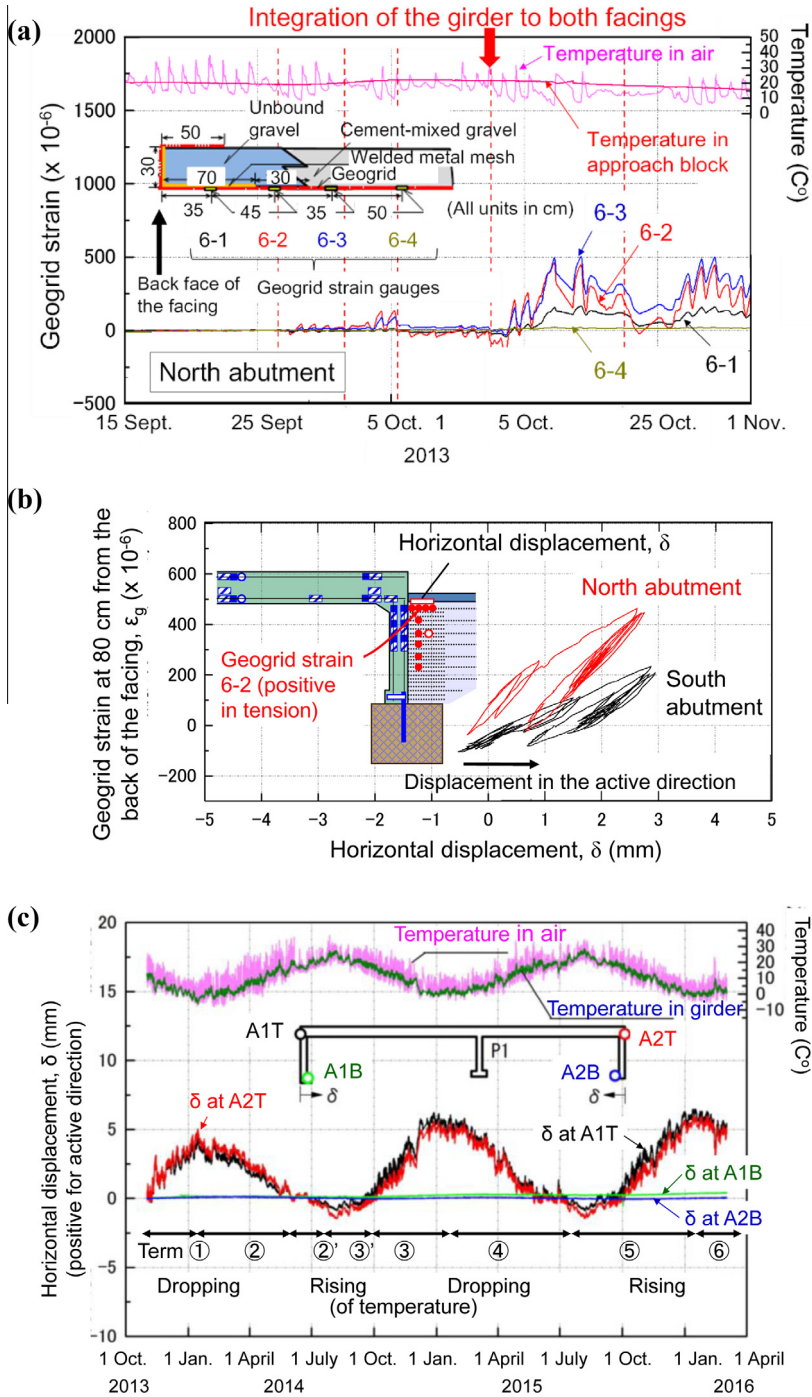


**Fig. 15.** Performance of GRS integral bridge at Haipe-sawa, Sanriku Railway: (a) and (b) during construction in the year of 2013 (Yamazaki et al., 2014); and (c)–(e) for a period of more than one year after completion.

$$\delta = \alpha \cdot \Delta t \cdot L \quad (1)$$

where  $\alpha$  is the linear thermal expansion coefficient =  $10^{-5}/^{\circ}\text{C}$ ;  $\Delta t$  is the temperature change from the start of observation (which is close to the temperature change from the moment when the girder was integrated to the facings); and  $L$  is the

girder length (60 m). The difference between the measured relations and this theoretical relation is due to the restraint at the ends of the girder by changes in the tensile forces in the geogrid reinforcement (which increases when  $\delta$  decreases associated with the active displacement of the facings and vice versa) and changes in the earth pressure

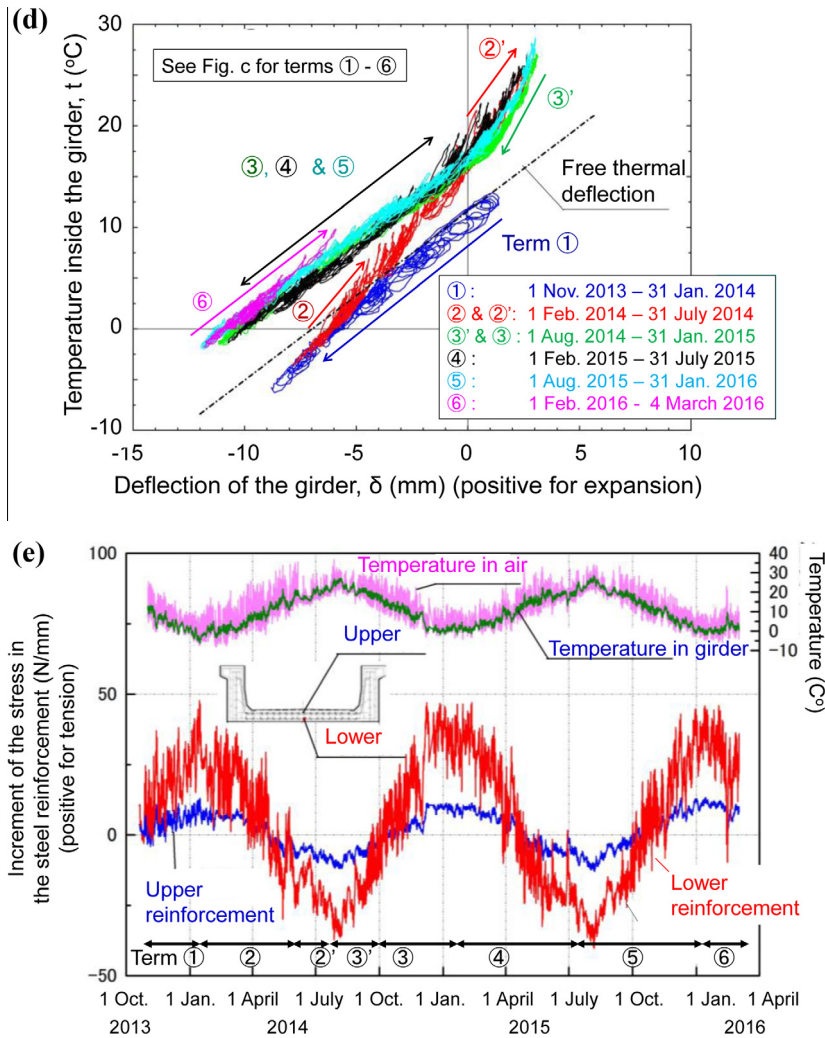


Fig. 15 (continued)

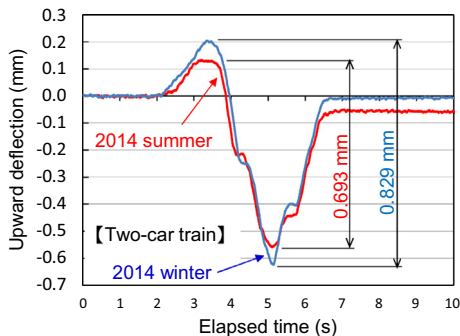
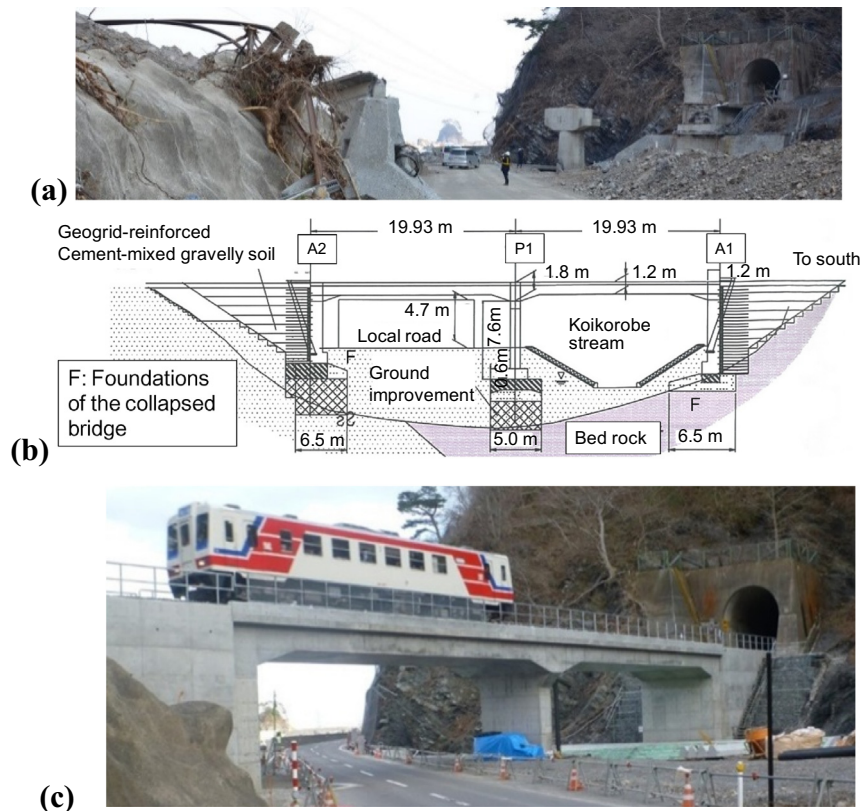


Fig. 16. Vertical deflection at the center of second (northern) span of Heipe-sawa GRS integral bridge by passing of a two-coach train at the end of August and the mid of December, 2014.

(which increases when  $\delta$  increases associated with the passive displacement of the facings and vice versa). The following trends of behaviour may be seen from Fig. 15d:

- (1) In terms 2' and 3',  $\delta$  is positive due to high temperature: i.e., the girder became longer than the one when the girder was integrated to the FHR facings. The slope of the relations in these terms is larger than the one under the free thermal deflection condition. This is due to the fact that the facings displaced in the passive mode relative to the initial condition, thus the coefficient of horizontal sub-grade reaction became higher.
- (2) In term 1, after  $\delta$  became negative (i.e., the girder became shorter than the value at the moment of integration) due to temperature drop, the thermal contraction rate was similar to the one under the free thermal deflection condition. It is likely therefore that the coefficient of horizontal sub-grade reaction in the active mode of the approach blocks was negligible or very small while the geogrid tensile resistance was also negligible or very low. After  $\delta$  became smaller about  $-6$  mm, the slope



**Fig. 17.** Koikorobe-sawa bridge, Sanriku Railway: (a) 30 March 2011; (b) structure of GRS integral bridge seen from the inland; and (c) completed (6th April 2014).

became larger than the one under the free thermal deflection conditions. It seems that the geogrid tensile resistance gradually started effective.

- (3) The rate of the thermal expansion of the girder in term 2 (when the temperature was rising) was smaller than the one under the free thermal deflection condition. This event was associated with slight parallel-shifting of the relation in term 1 to the one in term 3. It is likely that these trends would be a continuous decrease in  $\delta$  due to continuous shrinkage of the concrete of the girder probably by drying. This inference is supported by the fact that the minimum value of  $\delta$  in the second winter (at the end of term 3) is slightly larger than the one in the first winter (at the start of term 2): i.e., the length of the girder slightly decreased, which resulted in slight active displacements at the top of the facings. However, the relations in the latest terms 4, 5 and 6 during a period until the end of 4 March 2016 (when the temperature was rising) nearly perfectly overlap the relation in term 3. This fact indicates that the shrinkage of concrete by drying had ended nearly perfectly by the time when the manuscript of this paper was written (March 2016). The fact that the value of  $\delta$  at the same temperature is the same when the temperature is dropping and rising also indicates that the behaviour of the unbound gravelly soil zone

immediately behind the facing is now nearly perfectly reversible without exhibiting the ratcheting phenomenon (Tatsuoka et al., 2009, 2010b, 2012). If this phenomenon had taken place by cyclic lateral displacements at the top of the facings caused by cyclic temperature changes, it would have continuously increased the earth pressure on the back of the facing retaining unbound gravelly soil zones. Obviously, this phenomenon has not taken place at all in this case.

Fig. 15e shows the time histories of the increment of the stress in the steel reinforcement at the section M denoted in Fig. 13c (at the end of the horizontal haunch in front of the FHR facing of the north side abutment: i.e., the left abutment in this figure). The stress increment is defined zero at the time of the start of observation (i.e., close to the time when the girder was integrated to the FHR facings). When the girder shrinks due to a drop in the ambient temperature, steel reinforcement exhibits axial compression larger than that of concrete, therefore, the tensile strain in the steel reinforcement increases. The opposite phenomenon takes place when the girder expands due to a rise in the ambient temperature. Yet, the thermal strain changes in the steel reinforcement are insignificant, while the peak tensile strains in winter are very low.

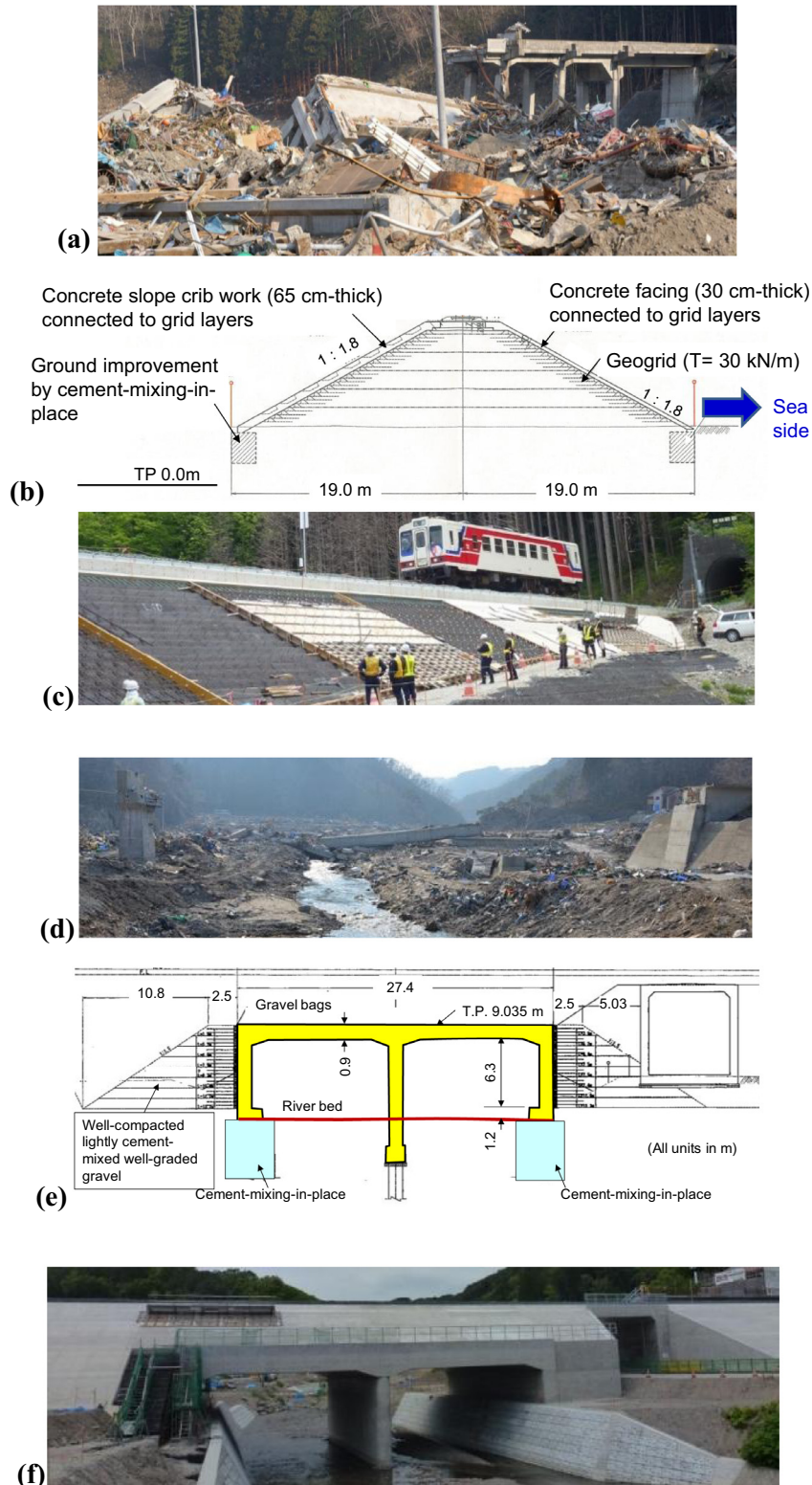


**Fig. 18.** Shimanokoshi, Sanriku Railway: (a) RC viaduct that collapsed by tsunami, seen from the inland (30th March 2011); (b) structure of GR embankment; (c) GR embankment seen from the inland (20 May 2014); (d) immediately after the earthquake, seen from the seaside (30th March 2011); (e) structure of GRS integral bridge; and (f) completed (20th May 2014).

Fig. 16 shows typical vertical deflection at the center of the northern span of Heipe-sawa GRS integral bridge when a two-coach train passed (as shown in Fig. 13e). The axle load of an empty coach is 80.5 kN, so the total weight of an empty coach is 320 kN. The measured deflections are substantially lower than the allowable limit, which is of the order of 30 mm determined to limit the tension crack of the girder concrete. A slightly smaller deflection in summer is due mainly to larger restraint of the approach fill resulting from a passive displacement of the facing in summer.

These measurements shown above indicate that the bridge has been highly stable.

#### *Koikorobe-sawa GRS integral bridge*

Another GRS integral bridge was constructed at Koikorobe-sawa to restore a two-span simple-supported girder bridge that was completely washed away by the great tsunami. Part of the previous foundations was utilized to construct this GRS integral bridge (Fig. 17b). The length of the girder is about 40 m, shorter than the one at Haipe-sawa. The thermal deflection of the girder is smaller for that reason. Besides, there is no specific spatial restriction below the girder. Therefore, a deck bridge with a RC girder was employed. The structure of the connection zone between the facing and the approach block immediately behind the facing is the same as the GRS integral bridge at Haipe, presented in Fig. 14b.

#### *GRS structures at Shimanokoshi*

The RC viaduct at Shimanokoshi fully collapsed by the tsunami (Fig. 18a). On the request of the residents at the site, geosynthetic-reinforced (GR) embankment was constructed as a tsunami barrier in place of the RC viaduct (Figs. 18b and c). Both slopes of the GR embankment are covered with lightly steel-reinforced concrete facing firmly connected to the geogrid layers reinforcing the backfill. In this way, a high seismic stability of embankment is ensured, while the panels placed on the top and slopes of the embankment can have a sufficient stability against a deep over-topping tsunami current.

At this site, a GRS integral bridge was also constructed (Figs. 18e and f) to restore a simple-supported girder bridge that fully collapsed by the tsunami (Fig. 18d). The GRS integral bridge is underlain by a backfill layer to reduce as much as possible the size of the opening.

It is to be emphasized that the focus of the case histories presented above is not only the satisfactory performance under extreme conditions. That is, although the first GRS bridge at Kikonai is for a high speed train, this technology was not developed exclusively for high speed trains but obviously this technology can be used for ordinary trains (as in the other case histories described in this paper) and also for highways and ordinary local roads. In addition, the other three GRS bridges were constructed to restore the bridges that collapsed by a great tsunami. Yet, as detailed in the paper, these bridges were designed not only to be stable enough under extreme loading condition (i.e., severe seismic loading, tsunami etc), but also to function satisfactorily under ordinary loading conditions for a long-term life period, as validated by the satisfactory

performance under ordinary loading conditions for a couple of years.

Finally, several other GRS integral bridges have been either completed or at the stage of design and research for longer spans than the one at Haipe that is currently underway. The outcome from the above will be reported elsewhere in the near future.

## Conclusions

GRS integral bridge was developed by extending the technology of GRS retaining wall having staged-constructed full-height rigid (FHR) facing. Compared with the conventional type bridge comprising a simple-supported girder (or girders), GRS integral bridge is much more cost-effective with a reduced period of construction and its performance is much higher with a low maintenance cost, negligible bumps behind the facing and a high stability during long-term service and against severe earthquakes, floods and tsunamis. These characteristic features can be attributed to the staged construction of FHR facing that is firmly connected to the geogrid layers and the structural integration of a continuous girder to the top of the FHR facings. For these reasons, GRS integral bridge is relevant for railways and roads at many places.

## References

- Abu-Hejleh N, Zornberg JG, Wang T, Watcharamonthein J. Monitored displacements of unique geosynthetic-reinforced soil bridge abutments. *Geosynth. Int.* 2002;9:71–95. NO. 1.
- Aoki H, Yonezawa H, Tateyama T, Shinoda M, Watanabe K. Development of aseismic abutment with geogrid-reinforced cement-treated backfill. In: *Proc. 16th IC on SMGE, Osaka*. p. 1315–8.
- Helwany SMB, Wu JTH, Froessl B. GRS bridge abutments—an effective means to alleviate bridge approach settlement. *Geotext. Geomembr.* 2003;21(3):177–96.
- Hirakawa D, Nojiri M, Aizawa H, Tatsuoka F, Sumiyoshi T, Uchimura T. Behaviour of geosynthetic-reinforced soil retaining wall subjected to forced cyclic horizontal displacement at wall face. In: *Proc. 8th Int. Conf. on Geosynthetics, Yokohama 2006*;3. p. 1075–8.
- Hirakawa D, Nojiri M, Aizawa H, Tatsuoka F, Sumiyoshi T, Uchimura T. Residual earth pressure on a retaining wall with sand backfill subjected to forced cyclic lateral displacements. In: Ling et al., editors. *Soil Stress-Strain Behavior: Measurement, Modeling and Analysis. Geotech. Symposium in Roma 2006*. p. 865–74.
- Horvath JS. Integral-abutment bridges: geotechnical problems and solutions using geosynthetics and ground improvement. In: *Proceedings of the 2005 FHWA Conference on Integral Abutment and Jointless Bridges, Baltimore, MD, USA; 2005*. p. 281–91.
- Kuwabe S, Kikuchi Y, Watanabe K, Tatsuoka F. Model tests on the stability of GRS integral bridge against tsunami load. In: *Proceedings of 15th Asian Regional Conference on Soil Mechanics and Geotechnical Engineering, Fukuoka; 2015*.
- Koda M, Nonaka T, Suga M, Kuriyama M, Tateyama M, Tatsuoka F. A series of lateral loading tests on a full-scale model of geosynthetic-reinforced soil integral bridge. In: Ling et al., editors. *Proc. Int. Sym. on Design and Practice of Geosynthetic-Reinforced Soil Structures, Bologna, Italy; 2013*. p. 157–74.
- Kuwano J, Koseki J, Miyata Y. Performance of reinforced soil walls in the 2011 Tohoku Earthquake. In: *Proc. 5th Asian Regional Conference on Geosynthetics, Bangkok, Thailand; 2012*. p. 85–94.
- Kuwano J, Koseki J, Miyata Y. Performance of reinforced soil walls during the 2011 Tohoku earthquake. *Geosynth Int* 2014;21(3):1–18.
- Lee KZZ, Wu JTH. A synthesis of case histories on GRS bridge-supporting structures with flexible facing. *Geotext Geomembr* 2004;22(4):181–204.
- Munoz H, Tatsuoka F, Hirakawa D, Nishikiori H, Soma R, Tateyama M, Watanabe K. Dynamic stability of geosynthetic-reinforced soil integral bridge. *Gesynth Int* 2012;19(1):11–38.

- Nagatani T, Tamura Y, Ojima M, Tateyama M, Kojima K, Watanabe K. Construction and field observation of the full-scale test integral GRS bridge. *Geosynth Eng J IGS Jpn Chapter 2009*;24:219–26 (in Japanese).
- RTRI (Railway Technical Research Institute). Design standards for railway structures and commentary: earth retaining structure, January 2012, edited under supervision of Railway Bureau of Ministry of Land, Transport and Tourism, Japanese Government (in Japanese); Infrastructure; 2012.
- Sasaki T, Nishioka H, Kojima K, Takano Y, Suyama Y, Aoki H. Behaviors of girder and backfill of GRS integral bridge focusing on tension force of geosynthetic. *J. Geosynth Eng IGS Jpn Chapter 2014*;29:205–8 (in Japanese).
- Shindo Y, Yamazaki T, Yonezawa T, Inoue S. Analysis of the tsunami-resistance of GRS integral bridge. In: *Proc. 70th Annual Meeting of Japanese Society for Civil Engineers, Okayama*; 2015 (in Japanese).
- Skinner GD, Rowe RK. Design and behaviour of a geosynthetic reinforced retaining wall and bridge abutment on a yielding foundation. *Geotext Geomembr 2005*;23(3):234–60.
- Suga M, Nonaka T, Kuriyama R, Kojima K, Koda M. A series of lateral loading test of the geosynthetic-reinforced soil integral bridge. *J Geosynth Eng IGS Jpn Chapter 2012*;27:157–64 (in Japanese).
- Tamura Y, Shiraiishi H, Suyama Y, Aoki H, Nishioka H, Kato H. Two-directional cyclic lateral loading tests on the facing of the GRS abutment of GRS integral bridge supporting a long girder (no. 1: outline of the test). In: *Proc. 4th National Conference, Japanese Geotechnical Society, Toyama, Paper No. 771*; 2013. p. 1541–2.
- Tatsuoka F. Roles of facing rigidity in soil reinforcing. In: *Proc. Earth Reinforcement Practice, IS-Kyushu 1992*;92. p. 831–70.
- Tatsuoka F, Watanabe K. Design, construction and performance of GRS structures for railways in Japan. In: *Indraratna Buddhima et al., editors. Ground Improvement Case Histories-Compaction. Grouting and geosynthetics. Elsevier*; 2015. p. 657–92.
- Tatsuoka F, Yamauchi H. A reinforcing method for steep clay slopes with a non-woven fabric. *Geotext Geomembr 1986*;4(3/4):241–68.
- Tatsuoka F, Tateyama M, Murata O. Earth retaining wall with a short geotextile and a rigid facing. In: *Proc. 12th Int. Conf. on SMFE, Rio de Janeiro 1989*;12. p. 1311–4.
- Tatsuoka F, Tateyama M, Uchimura T, Koseki J. Geosynthetics-reinforced soil retaining walls as important permanent structures, 1996–1997 mercer lecture. *Geosynth Int 1997a*;4(2):81–136.
- Tatsuoka F, Koseki J, Tateyama M. Performance of reinforced soil structures during the 1995 Hyogo-ken Nanbu Earthquake. In: *Special Lecture, International Symposium on Earth Reinforcement (IS Kyushu '96), Balkema 1997b*;2. p. 973–1008.
- Tatsuoka F, Koseki J, Tateyama M, Munaf Y, Horii N. Seismic stability against high seismic loads of geosynthetic-reinforced soil retaining structures. In: *Keynote Lecture, Proc. 6 ICG, Atlanta 1998*;1. p. 103–42.
- Tatsuoka F, Tateyama M, Tamura Y, Yamauchi H. Lessons from the failure of full-scale models and recent geosynthetic-reinforced soil retaining walls. In: *Proc. the second Asian Geosynthetics Conference, GeoAsia 2000, Kuala Lumpur 2000a*;1. p. 23–53.
- Tatsuoka F, Tateyama M, Tamura Y, Yamauchi H. Lessons from the failure of full-scale models and recent geosynthetic-reinforced soil retaining walls. In: *Proc. Second Asian Geosynthetics Conference, GeoAsia 2000, Kuala Lumpur 2000b*;1. p. 23–53.
- Tatsuoka F, Tateyama M, Aoki H, Watanabe K. Bridge abutment made of cement-mixed gravel backfill. In: *Indraratna, Chu, editors. Ground Improvement, Case Histories. Elsevier Geo-Engineering Book Series 2005*;vol. 3. p. 829–73.
- Tatsuoka F, Hirakawa D, Nojiri M, Aizawa H, Tateyama M, Watanabe K. Integral bridge with geosynthetic-reinforced backfill. In: *Proc. 1st Pan American Geosynthetics Conference & Exhibition, Cancun, Mexico*; 2008. p. 1199–208.
- Tatsuoka F, Hirakawa D, Nojiri M, Aizawa H, Nishikiori H, Soma R, Tateyama M, Watanabe K. A new type of integral bridge comprising geosynthetic-reinforced soil walls. *Geosynth Int 2009*;16(4):301–26.
- Tatsuoka F, Hirakawa D, Nojiri M, Aizawa H, Nishikiori H, Soma R, Tateyama M, Watanabe K. Closure to discussion on “a new type of integral bridge comprising geosynthetic-reinforced soil walls”. *Geosynth Int 2010a*;17(4):1–12.
- Tatsuoka F, Koseki J, Tateyama M. Introduction to Japanese codes for reinforced soil design. In: *Panel Discussion on Reinforced Soil Design Standards, Proc. 9th International Conference on Geosynthetics, Brazil*; 2010. p. 245–55.
- Tatsuoka F, Tateyama M, Koseki J. GRS structures recently developed and constructed for railways and roads in Japan, Keynote lecture. In: *Miura et al., editors. Proc. Second International Conference on Transportation Geotechnics (IS-Hokkaido 2012)*; 2012. p. 63–84.
- Tatsuoka F, Tateyama M, Koseki J, Yonezawa T. Geosynthetic-Reinforced Soil Structures for Railways in Japan. *Trans Infrastruct Geotechnol 2014a*;1(1):3–53. Springer.
- Tatsuoka F, Tateyama M, Koda M, Watanabe K, Koseki J, Aoki H, Yonezawa T. Design, construction and performance of GRS structures for railways in Japan. In: *Proc. 10th International Conference on Geosynthetics, Berlin, September*; 2014.
- Tatsuoka F, Koseki J, Kuwano J. Natural disasters mitigation by using construction methods with geosynthetics (earthquakes), Keynote Lecture. In: *Proc. 10th International Conference on Geosynthetics, Berlin, September*.
- Tatsuoka F, Tateyama M, Koda M, Kojima K, Yonezawa T, Shindo Y, Tamai S. Recent research and practice of GRS integral bridges for railways in Japan. In: *Proceedings of 15th Asian Regional Conference on Soil Mechanics and Geotechnical Engineering, Fukuoka*; 2015.
- Thamm BR, Krieger B, Krieger J. Full-scale test on a geotextile reinforced retaining structure. In: *Prof. 4th Int. Conf. on Geotextiles, Geomembranes and Related Products 1990*;1. p. 3–8.
- Thamm BR, Krieger B, Lesniewska D. Full-scale test on a geotextile reinforced soil wall. In: *McGown et al., editors. Performance of Reinforced Soil Structures. Thomas Telford*; 1991. p. 341–5.
- Yamazaki T, Shindo Y, Kojima K, Sasaki T. Study of measurement results of GRS integral bridge in Sanriku railway, Kita-riusu Line. *J Geosynth Eng IGS Jpn Chapter 2014*;29:201–4 (in Japanese).
- Yazaki S, Tatsuoka F, Tateyama M, Koda M, Watanabe K, Duttine A. Seismic design of GRS integral bridge. In: *Ling et al., editors. Proc. International Symposium on Design and Practice of Geosynthetic-Reinforced Soil Structures, Bologna, Italy*; October 2013. p. 142–56.
- Yonezawa T, Yamazaki T, Tateyama M, Tatsuoka F. Design and construction of geosynthetic-reinforced soil structures for hokkaido high-speed train line. *Trans Geotech 2014*;1(1):3–20. Elsevier.
- Zornberg JG, Abu-Hejleh N, Wang T. Measuring the performance of geosynthetic reinforcement in a Colorado bridge structure. *GFR Mag (Geosynthetics) 2001*;19(2). Industrial Fabric Association International.